



Original

RNA-Seq analysis of obese *Pdha1^{fl/fl}*Lyz2-Cre mice induced by a high-fat diet

Zhaohong GENG^{1)*}, Yuchan YUAN^{2)*}, Dan HE³⁾, Hewang LEE⁴⁾, Hongyan WANG¹⁾, Nan NIU¹⁾, Zhigang NI¹⁾, Shopit ABDULLAH⁵⁾, Zeyao TANG⁵⁾ and Peng QU¹⁾

¹⁾Department of Cardiology, Second Affiliated Hospital of Dalian Medical University, No. 467 Zhongshan Road, Dalian 116000, P.R. China

²⁾Department of Cardiology, Xinhua Hospital Affiliated to Shanghai Jiaotong University School of Medicine, 1665 Kongjiang Road, Shanghai, 200092, China

³⁾Department of Cardiology, Peking University People's Hospital, No. 11, Xizhimen South Street, Xicheng District, Beijing, 100044, P.R. China

⁴⁾Kidney Disease Section, Kidney Diseases Branch, National Institute of Diabetes and Digestive and Kidney Diseases, National Institutes of Health, 9000 Rockville Pike, Bethesda, MD 20892, USA

⁵⁾Academic Integrated Medicine & College of Pharmacy, Department of Pharmacology, Dalian Medical University, No. 9 West Section Lvshun South Road, Dalian 116044, P.R. China

Abstract: Pyruvate dehydrogenase complex (PDH) is an important complex of three enzymes that transforms pyruvate into acetyl-CoA, subsequently entering the tricarboxylic acid (TCA) cycle to produce ATP and electron donors. As a key regulator of energy and metabolic homeostasis, PDH is considered a potential therapeutic target of many diseases. On the other hand, the relationship between PDH and obesity is not clear. In this study, peripheral blood of *Pdha1^{fl/fl}*Lyz2-Cre and C57BL/6 mice fed a high-fat diet (HFD) was collected and subjected to extensive transcriptome sequencing. Differentially expressed genes (DEGs) were identified. Enrichment of functions and signaling pathways analyses were performed based on Gene Ontology (GO) and the Kyoto Encyclopedia of Genes and Genomes (KEGG) database. Quantitative real-time polymerase chain reaction (qRT-PCR) was used to verify the genes selected from RNA sequencing (RNA-seq). Eventually, we found that *Pdha1^{fl/fl}*Lyz2-Cre mice were more susceptible to HFD-induced obesity. A total of 302 up-regulated genes and 30 down-regulated genes were screened that were differentially expressed between *Pdha1^{fl/fl}*Lyz2-Cre mice fed the HFD and the control groups. Furthermore, we verified that significant transcriptional changes in the genes *Sgstm1*, *Ncoa4*, *Rraga*, *Slc3a2*, *Usp15*, *Gabarapl2*, *Wipi1*, *Sh3glb1*, *Mtmt3*, and *Cd36* were consistent with the results obtained from RNA-seq analysis. In summary, this study preliminarily established that there is a close relationship between *Pdha1* and obesity and revealed the possible downstream pathways and target genes involved, laying a good foundation for the further study of *Pdha1* function in the future.

Key words: knockout mice, obesity, *Pdha1*, RNA-seq

Introduction

With the material wealth in modern society, the high-fat diet is becoming a popular dietary style. However, such inappropriate long-term eating habits may cause

many health problems, among which obesity is the most prominent. Obesity is now reported to be one of the important causes of several immune and metabolic diseases, such as cardiovascular diseases, diabetes, and some cancers [1, 2]. Adipose tissue, which is closely

(Received 13 April 2022 / Accepted 20 September 2022 / Published online in J-STAGE 25 October 2022)

Corresponding authors: Z. Tang. email: tangzeyao@aliyun.com

P. Qu. email: qupeng777@aliyun.com

*These authors contributed equally to this work.



This is an open-access article distributed under the terms of the Creative Commons Attribution Non-Commercial No Derivatives (by-nc-nd) License <<http://creativecommons.org/licenses/by-nc-nd/4.0/>>.

©2023 Japanese Association for Laboratory Animal Science

associated with obesity, secretes many adipokines, leading to many kinds of metabolic processes [3]. Obesity is also relevant to inflammation, which is characterized by the accumulation of immune cells and inflammatory and metabolic mediators at multiple organ sites [4, 5]. Furthermore, macrophages, as a central part of the innate immune system, have been closely associated with the pathogenesis of obesity [6]. Significant changes in quantity and polarization state of macrophages may be responsible for the onset and development of obesity. Macrophages release inflammatory mediators that can act within adipose tissue, promoting adipose cell hypertrophy and death. Adipose tissues secrete inflammatory chemokines, promoting macrophage recruitment and M1 polarization. The above interactions form a malignant cycle, which promotes local or systemic inflammation, adipose tissue remodeling, liver damage, and insulin resistance, eventually leading to obesity and related complications. Thus, macrophages are one of the crucial cell types responsible for maintaining homeostasis and regulating inflammatory and regenerative processes. The accumulation of metabolites is considered to be the result of dysfunction of the tricarboxylic acid cycle (TCA) [7]. Macrophages then exhibit different phenotypes and functions according to the microenvironment changes [8]. Classically activated macrophages exhibit pro-inflammatory properties mainly caused by glycolysis, while alternatively activated macrophages are associated with the oxidative phosphorylation system (OXPHOS) driven anti-inflammatory processes.

Pyruvate dehydrogenase complex (PDH) is the most important complex of the three enzymes that convert pyruvate into acetyl coenzyme A, subsequently entering the TCA cycle to produce ATP and electron donors. PDH consists of E1, E2, and E3 components. The decarboxylation of pyruvate is catalyzed by pyruvate dehydrogenase E1 component subunit alpha (PDHA1), which is considered to be a rate-limiting reaction [9]. As a key regulator of energy and metabolic homeostasis, PDH is considered as a potential therapeutic target. Some evidence suggests pyruvate dehydrogenase kinase isoform 4 (PDK4), which inhibits PDH, plays key roles in cell energy balance, mitochondrial injury, endoplasmic reticulum stress, inflammation, autophagy, apoptosis, and calcium balance [10]. Also, PDK4 is closely related to mitochondrial function in vascular smooth muscle cells (VSMCs) [11]. Dichloroacetate (DCA), a well-established PDH activator, can reduce atherosclerosis in ApoE^{-/-} mice [12]. As PDH plays an important role in cell energy metabolism, systemic knockout PDH mice are prone to death. Looking at the current literature, there is a lack of suitable animal models to study the biological

effects of PDH.

In this paper, we constructed mice with a specific *Pdhal* defect in macrophages (*Pdhal*^{f/f}Lyz2-Cre) to determine whether *Pdhal*^{f/f}Lyz2-Cre mice are sufficient to reproduce the phenotype changes observed in obesity and performed an RNA sequencing (RNA-seq) analysis of blood to compare global gene expression between *Pdhal*^{f/f}Lyz2-Cre mice with obesity induced by a high-fat diet (HFD) and controls. Additionally, the differentially expressed genes between these two groups were analyzed to determine the enriched pathways. Based on the experimental results, we preliminarily studied the effect of PDH on the characterization of obesity in mice with obesity induced by an HFD.

Materials and Methods

Pdhal^{f/f}Lyz2-Cre mouse construction

CRISPR technology was used to cut the DNA of the target gene intron. Cas9 nickase, *Pdhal*-L (TGGATTG-GTTATGGTTTCTGG), and *Pdhal*-R (CCAAAGTGC-CACGCCAGAAGG) were transcribed into mRNA and RNA *in vitro*, which were then microinjected into the fertilized eggs of mice with donor DNA to obtain gene knockin mice efficiently. Gene knockout occurs in the early stages of the development of zygotes or even at the single-cell stage, thus the rate of chimerism and probability of seed transmission in mice are high.

Gene knockout was realized by direct injection of zygotes. Two weeks after the birth of mice, tails were cut, and genomic DNA was extracted for PCR and then sequenced to detect the genotypes of the mice and whether accurate insertion of floxp at two sites was achieved. Eventually, *Pdhal*-floxp was inserted at both ends of specific exons. Then, *Pdhal*-floxp mice were mated with Lyz2-Cre mice, resulting in the deletion of specific exons of *Pdhal*, no translation or frameshift mutation of *Pdhal*, and inactivation of PDHA1 protein and achieving the purpose of conditional knockout of the *Pdhal* gene (Figs. 1A and B), which may also be useful for Cre-lox studies of the myeloid cell lineage. The *Pdhal*^{f/f}Lyz2-Cre mice were constructed by Beijing Viewsolid Biotech Co., Ltd. The animal experiments were approved by the ethics committee of Dalian Medical University.

Animal experiments and physiological measurements

Male wild-type (WT) and *Pdhal*^{f/f}Lyz2-Cre mice that were 8 to 12 weeks old were housed in a room at a constant temperature of around 22°C with a 12 h light/dark cycle and allowed free access to food and water. Age-matched mice were given either a low-fat diet or HFD.

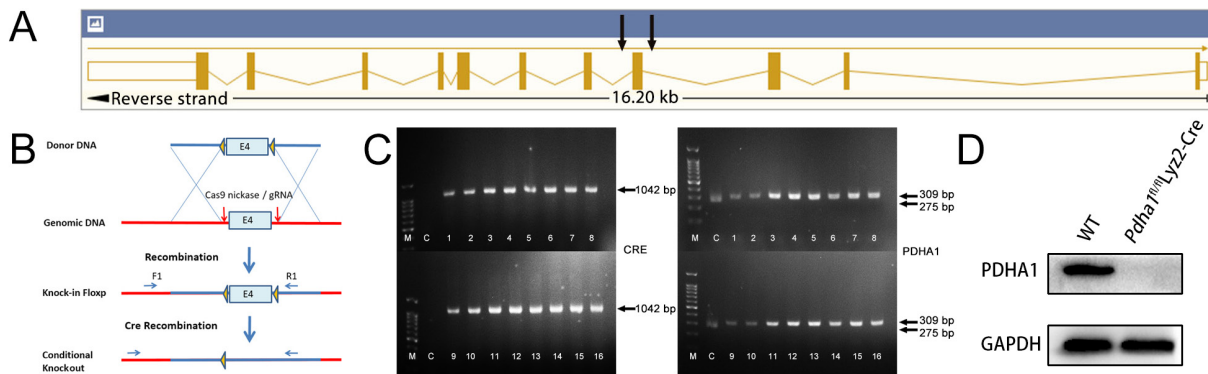


Fig. 1. *Pdha1^{fl/fl}Lyz2-Cre* mice were constructed to achieve conditional *Pdha1* knockout. A. Genome structure of the *Pdha1* transcription product. B. Principles of the *Pdha1^{fl/fl}Lyz2-Cre* mouse construction technology. C. Genotyping of *Pdha1^{fl/fl}Lyz2-Cre* mice. D. Peritoneal macrophages were isolated from wild-type (WT) and *Pdha1^{fl/fl}Lyz2-Cre* mice. The expression of pyruvate dehydrogenase E1 component subunit alpha (PDHA1) was detected by western blot (WB) method.

After 4 weeks, the mice were put into clean cages and fasted for more than 12 h. Body weight was measured every week for each mouse. An intraperitoneal glucose tolerance test (IPGTT) was performed on the 21st day. Blood samples were collected via the orbital venous plexus using a capillary glass tube. Some blood samples were mixed with 6 ml of TRIzol (TransGen Biotech, Beijing, China), shaken vigorously, and mixed for 1–2 min until the flocculent dissolved completely. Other blood samples were centrifuged, and the plasma was collected and stored at -80°C until analysis. The serum levels of triglyceride (TG), total cholesterol (TC), high-density lipoprotein (HDL), and low-density lipoprotein (LDL) were analyzed with a serum lipid assay kit (Nanjing Jiancheng Bioengineering Institute, Nanjing, China). Epididymal visceral adipose tissue and livers were obtained carefully and fixed in 4% paraformaldehyde for histological analysis. Peritoneal macrophages were collected from mice injected with 2 ml of 3% thioglycollate broth medium for 72 h. The expression of PDHA1 was detected by western blot (WB).

RNA-seq analysis

The degradation and contamination of peripheral blood RNA were monitored on 1% agarose gels. RNA purity was checked using a NanoPhotometer spectrophotometer (Implen, Westlake Village, CA, USA). RNA integrity was assessed using an Agilent 2100 Bioanalyzer system (Agilent Technologies, Santa Clara, CA, USA). A total of 1 μg RNA per sample was used as input material for the RNA sample preparations. Sequencing libraries were obtained using a NEBNext[®] Ultra[™] RNA Library Prep Kit for Illumina[®] (New England Biolabs, Ipswich, MA, USA) according to the manufacturer's recommendations, and index codes were added to attribute sequences to each sample. Clustering of the in-

dex-coded samples was performed on a cBot Cluster Generation System using TruSeq PE Cluster Kit v3-cBot-HS (Illumina) according to the manufacturer's instructions. After cluster generation, the library preparations were sequenced on an Illumina Novaseq platform, and 150 bp paired-end reads were acquired. Clean reads were obtained by removing reads containing adapters, reads containing ploy-N, and low-quality reads from raw data. Hisat2 v2.0.5 was used to build an index of the reference genome and to align paired-end clean reads to the reference genome. RNA-seq raw data were deposited in National Center for Biotechnology Information (NCBI) Sequence Read Archive (SRA) database under the accession number PRJNA 871785. Differential expression analysis of two groups (WT high fat vs *Pdha1^{fl/fl}Lyz2-Cre* high fat) was performed with the DESeq2 R package (1.16.1). Gene Ontology (GO) enrichment analysis of differentially expressed genes and testing of the statistical enrichment of differential expression genes in Kyoto Encyclopedia of Genes and Genomes (KEGG) pathways were performed with the clusterProfiler R package. The GO database describes the gene products in terms of functions, biological pathways, and cell localization, that is, simply annotating the gene products. KEGG is a database integrating genomic, chemical, and systemic functional information. One of the features of the KEGG database is that it links the gene catalog obtained from the fully sequenced genome with the system functions at the higher levels of the cell, species, and ecosystem.

Quantitative real-time polymerase chain reaction (qRT-PCR) analysis

Total RNA was extracted from peripheral blood of mice from each group using TRIzol reagent (TransGen Biotech). Synthesis of cDNA from total RNA, including

Table 1. Sequences of primers in this study

| Gene | GenBank accession number | | Sequence (5' → 3') |
|----------------|--------------------------|--|---|
| <i>Sgstm1</i> | NM_011018.3 | m- <i>Sgstm1</i> -F m- <i>Sgstm1</i> -R | TCCCAATGTCAATTTCTGAAGA TCTGTGCTGTGCTGGAAC |
| <i>Ncoa4</i> | NM_019744.4 | m- <i>Ncoa4</i> -F m- <i>Ncoa4</i> -R | CGCCAGACCATCACCACAT TGTGCCACTGGATGCTGACT |
| <i>Rraga</i> | NM_178376.3 | m- <i>Rraga</i> -F m- <i>Rraga</i> -R | GCGGCCAGGACACCTTAT GGATGGCTTCCAGACACGAT |
| <i>Slc3a2</i> | NM_001161413.1 | m- <i>Slc3a2</i> -F m- <i>Slc3a2</i> -R | GGGATGTGGGAAAGCTGATG GGTCGCTGGTGGATTCAAGT |
| <i>Usp15</i> | NM_027604.4 | m- <i>Usp15</i> -F m- <i>Usp15</i> -R | GGACTGGGACCCTGACTTGAA AGCTTCTCCTTGGTGGTGAAGA |
| <i>Gabap12</i> | NM_026693.5 | m- <i>Gabap12</i> -F m- <i>Gabap12</i> -R | TCATGTGGATCATCAGGAAAAGG TGTAGGCCACATACAAGAATCCAT |
| <i>Wipi1</i> | NM_145940.2 | m- <i>Wipi1</i> -F m- <i>Wipi1</i> -R | GGAGACCGTGCACATCTTCA GCCCTGTCTGGTTCATCAT |
| <i>Sh3glb1</i> | NM_001282037.1 | m- <i>Sh3glb1</i> -F m- <i>Sh3glb1</i> -R | CCATCATCTCCGCTGTCTGA ACTGGTGTCCCAGAGGTCTGA |
| <i>Mtmr3</i> | NM_001373897.1 | m- <i>Mtmr3</i> -F m- <i>Mtmr3</i> -R | GTGATCAGCGACCAGTGCTAGT GGCCAAAATCGAGCCATTC |
| <i>Cd36</i> | NM_001159558.1 | m- <i>Cd36</i> -F m- <i>Cd36</i> -R | GCAGCCTCCTTCCACCTTT AAAGGCATTGGCTGGAAGAA |
| <i>GAPDH</i> | NM_001289726.1 | m- <i>GAPDH</i> -F m- <i>GAPDH</i> -R | CAGGTTGTCTCCTGCGACTT GCCTCTTGTCTCAGTGTCC |

miRNAs with artificial poly (A) tails, was carried out using a PrimeScript II Fidelity Real Time-Polymerase Chain Reaction Kit (Solarbio® Life Sciences, Beijing, China). qRT-PCR was performed with Applied Biosystems 7500 FAST Real-time PCR Systems. The qRT-PCR primers were constructed as shown in Table 1.

Results

Pdha^{fl/fl}Lyz2-Cre mice are more susceptible to HFD-induced obesity

We successfully constructed the *Pdha*^{fl/fl}Lyz2-Cre mice (Figs. 1C and D). *Pdha*^{fl/fl}Lyz2-Cre mice could reproduce the phenotype changes in obesity. They also had significantly higher body weight gains and higher body masses than the WT controls. (Figs. 2A and B). Additionally, they showed an increase in blood glucose and area under the curve of the insulin tolerance test (AUC of ITT) compared with the WT controls (Figs. 2C and D). There were significant differences in TG, TC, and LDL-C between the WT low-fat and KO low-fat groups, while there was no significant difference in HDL between the WT low-fat and KO low-fat groups (Figs. 2E–H). Compared with the WT controls, *Pdha*^{fl/fl}Lyz2-Cre mice also manifested with significant increases in epididymal visceral adipose tissue (Fig. 3A). Histological staining of epididymal visceral adipose tissue showed an obvious reduction in the size of cells in white adipose tissue (WAT; Figs. 3B and C). *Pdha*^{fl/fl}Lyz2-Cre mice

manifested with adipose accumulation in liver tissue (Fig. 3D).

Differentially expressed gene (DEG) identification and GO and KEGG analyses

Clean reads used in subsequent analyses were obtained after original data filtering, a sequencing error rate check, and a GC content distribution check. The results are shown in Table 2. In total, 302 up-regulated and 30 down-regulated genes were screened between *Pdha*^{fl/fl}Lyz2-Cre mice a fed HFD and the control group. Clustering analysis showed that the gene expression levels displayed a higher clustering among the same group (Fig. 4A). We choose the top of the list to display (Table 3). Thirty significantly enriched GO terms were identified (Fig. 4B), with 10 related to biological processes, 10 related to cellular components, and 10 related to molecular functions. The biological process category contained cytolysis, erythrocyte homeostasis, defense response to other organism, transition metal ion homeostasis, myeloid cell homeostasis, defense response to virus, response to virus, glutathione metabolic process, iron ion homeostasis, and erythrocyte differentiation. The cellular component category contained outer membrane, organelle outer membrane, mitochondrial membrane part, respiratory chain complex IV, mitochondrial outer membrane, autophagosome membrane, organelle inner membrane, mitochondrial inner membrane, autolysosome, and secondary lysosome. The molecular func-

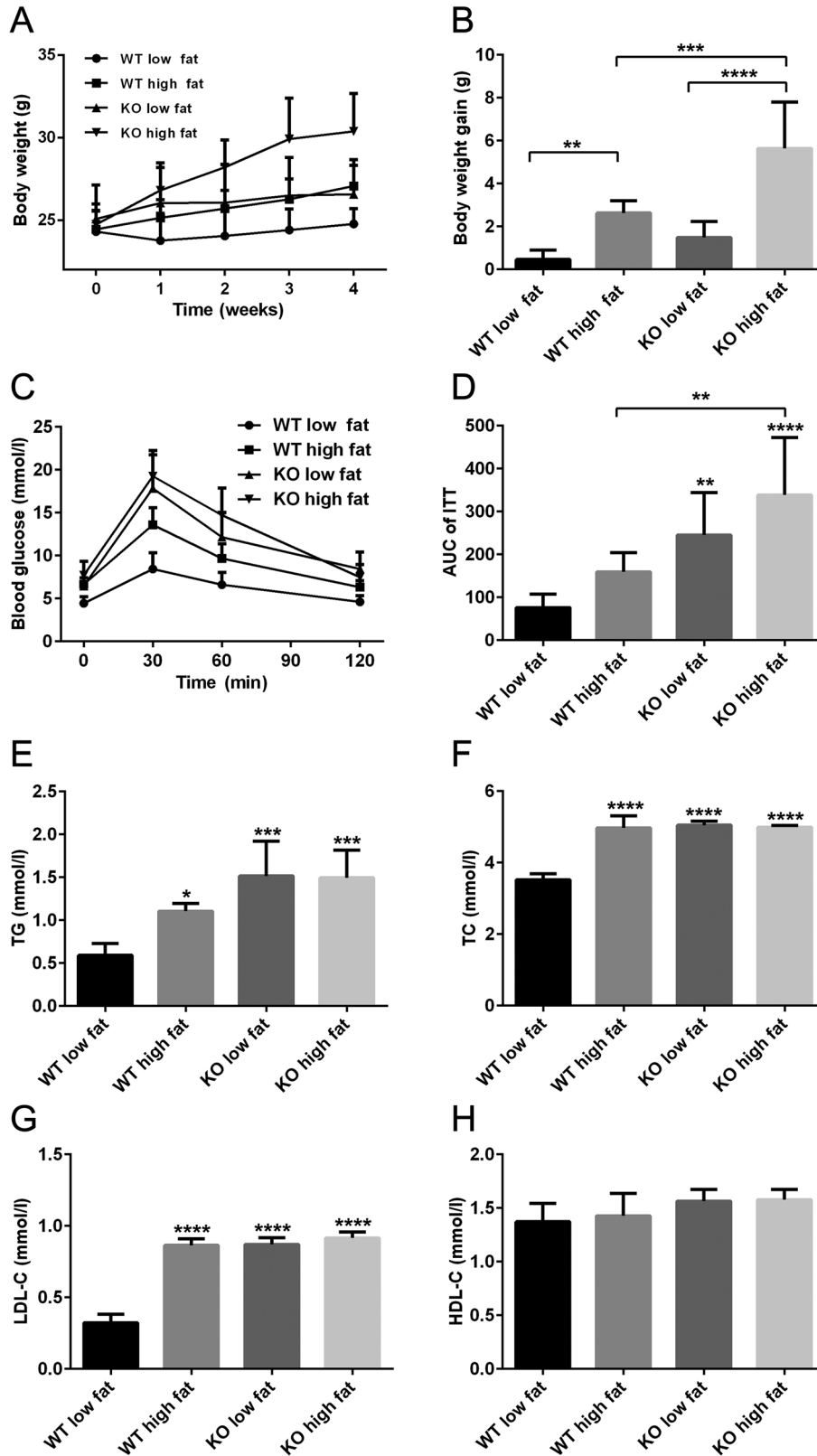


Fig. 2. Effect of *Pdha1^{fl/fl}Lyz2-Cre* mice on body weight gain, glucose, and serum lipids (n=8). WT low fat: wild-type mouse low-fat diet group. KO low fat: *Pdha1^{fl/fl}Lyz2-Cre* mouse low-fat diet group. WT high fat: wild-type mouse high-fat diet (HFD) group. KO high fat: *Pdha1^{fl/fl}Lyz2-Cre* mouse HFD group. A. Body weight. B. Body weight gain. C. Blood glucose. D. AUC of ITT. E. TG. F. TC. G. LDL-C. H. HDL-C. Data are presented as mean \pm SEM values (n=8). Significant differences among the groups were assessed by one-way ANOVA with Tukey's post hoc test. * $P < 0.05$, ** $P < 0.01$, *** $P < 0.001$, **** $P < 0.0001$.

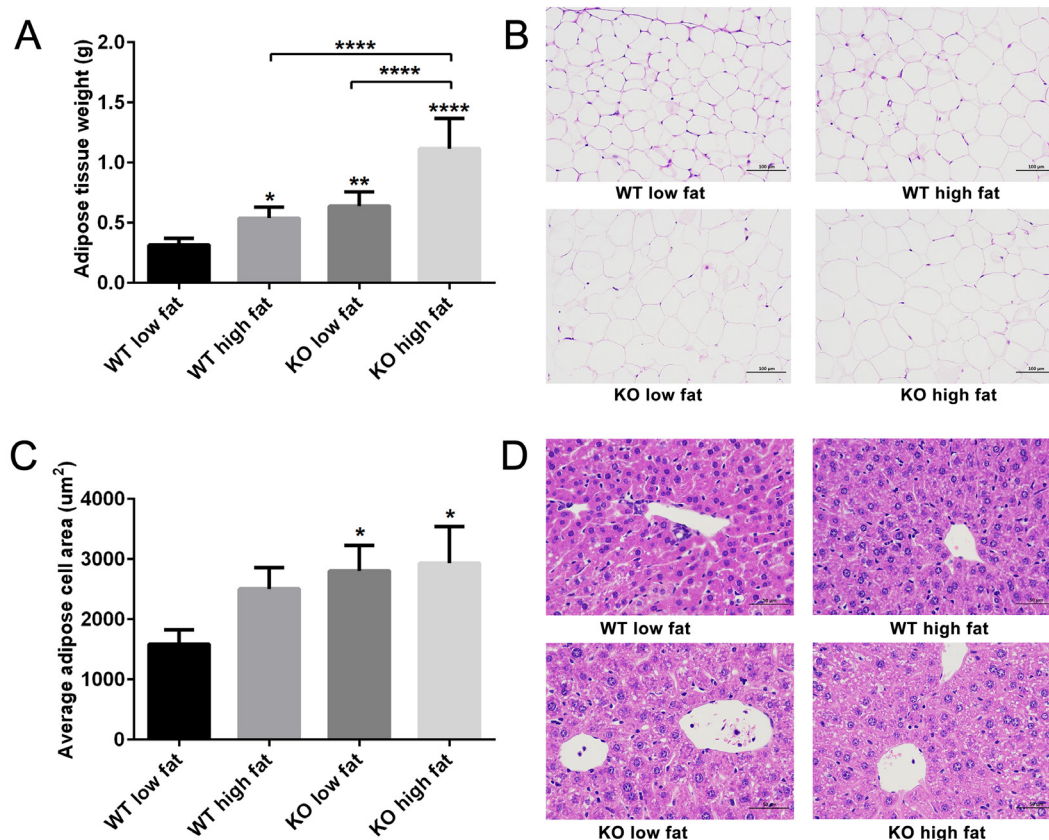


Fig. 3. Effect of *Pdhal*^{fl/fl}Lyz2-Cre mice on adipose tissue and the liver (n=8). WT low fat: wild-type mouse low-fat diet group. KO low fat: *Pdhal*^{fl/fl}Lyz2-Cre mouse low-fat diet group. WT high fat: wild-type mouse high-fat diet (HFD) group. KO high fat: *Pdhal*^{fl/fl}Lyz2-Cre mouse HFD group. A. Weight of epididymal visceral adipose tissue. B. Representative hematoxylin and eosin (H&E) staining of epididymal visceral adipose tissue. C. Adipocyte size. D. Representative H&E staining of the liver. Data are shown as mean ± SD values (n=8). Significant differences among the groups were assessed by one-way ANOVA with Tukey's post hoc test. **P*<0.05, ***P*<0.01, ****P*<0.001, *****P*<0.0001.

Table 2. Sequencing data quality

| Sample | Raw_reads ^{a)} | Clean_reads ^{b)} | Clean_bases ^{c)} | Error_rate ^{d)} | Q20 ^{e)} | Q30 ^{e)} | GC_pct ^{f)} |
|--------|-------------------------|---------------------------|---------------------------|--------------------------|-------------------|-------------------|----------------------|
| WT_HF1 | 91534320 | 84620852 | 12.69G | 0.02% | 98.24% | 95.07% | 56.30% |
| WT_HF2 | 106114044 | 94507134 | 14.18G | 0.02% | 98.23% | 95.02% | 55.51% |
| WT_HF3 | 87341524 | 77443058 | 11.62G | 0.02% | 98.13% | 94.77% | 56.29% |
| KO_HF1 | 79030006 | 68131758 | 10.22G | 0.02% | 98.08% | 94.54% | 55.19% |
| KO_HF2 | 83612766 | 74033794 | 11.11G | 0.02% | 98.33% | 95.13% | 55.30% |
| KO_HF3 | 109639270 | 98271728 | 14.74G | 0.02% | 98.44% | 95.46% | 56.97% |

^{a)}Number of total reads in original sequencing data. ^{b)}Number of reads after the quality control. ^{c)}Number of bases (G) after the quality control. ^{d)}Average sequencing error rate of clean reads. ^{e)}Proportion of the bases with a quality value over 20 or 30. If the error probability of one base is 0.001, then its Phred quality score is Q30. Similarly, if the error probability of one base is 0.01, its Phred quality score is Q20. ^{f)}Ratio of GC to total bases (clean data) in the sequencing data.

tion category contained carbon-sulfur lyase activity, neutral amino acid transmembrane transporter activity, amino acid transmembrane transporter activity, cytochrome-c oxidase activity, heme-copper terminal oxidase activity, oxidoreductase activity, acting on a heme group of donors, oxygen as acceptor, oxidoreductase activity, acting on a heme group of donors, antioxidant activity, lamin binding, and organic acid transmembrane transporter activity. Twenty significantly enriched KEGG

pathways were also identified (Fig. 4C). These pathways involved ferroptosis, mitophagy-animal, cardiac muscle contraction, ECM-receptor interaction, glutathione metabolism, ubiquitin mediated proteolysis, hematopoietic cell lineage, nitrogen metabolism, ether lipid metabolism, protein digestion and absorption, GABAergic synapse, drug metabolism-cytochrome P450, alcoholism, metabolism of xenobiotics by cytochrome P450, autoimmune thyroid disease, allograft rejection, autophagy-

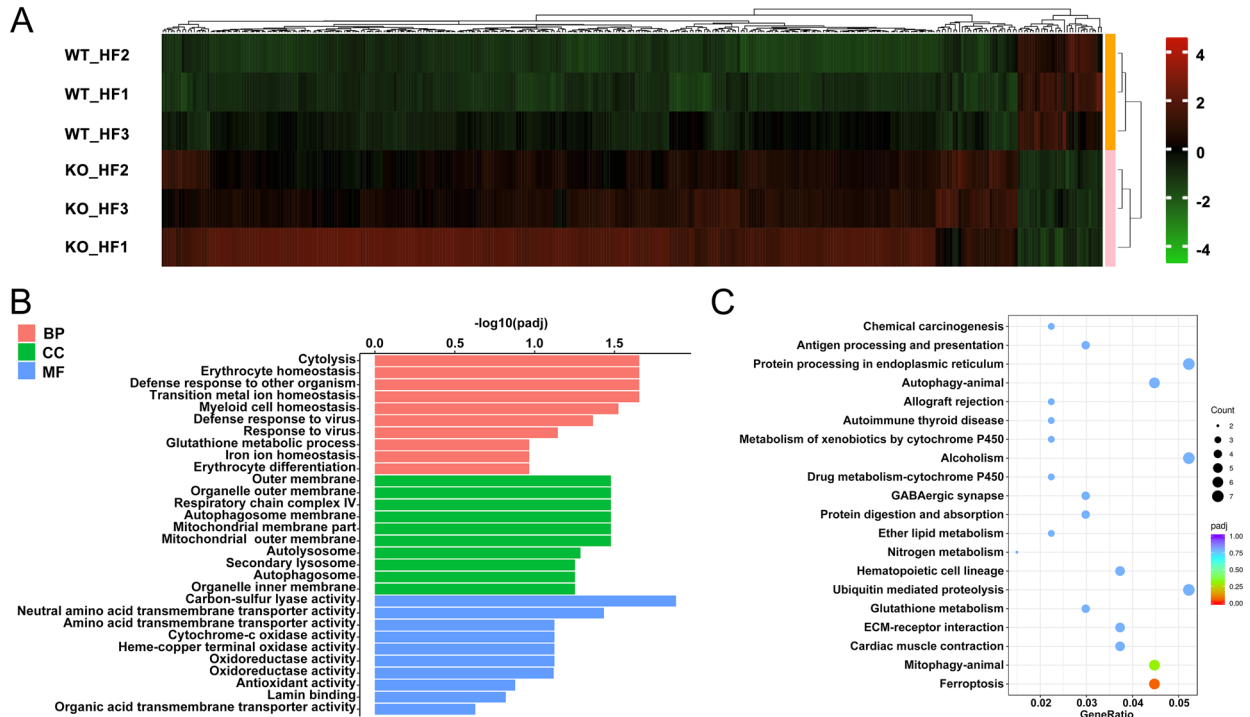


Fig. 4. RNA-seq of the blood from obese *Pdha1^{fl/fl}Lyz2-Cre* mice and wild-type (WT) mice (n=3). WT_HF: wild-type mouse high-fat diet (HFD) group. KO_HF: *Pdha1^{fl/fl}Lyz2-Cre* mouse HFD group. A. Heat map of the hierarchical clustering analysis. The ordinate is the sample name, and the abscissa is the normalized value of the differential gene FPKM. The redder the color is, the higher the expression level is; the greener the color is, the lower the expression level is. B. Gene Ontology (GO) analysis. The abscissa is the GO term, defining and describing the function of the gene product, and the ordinate is the significance level of GO term enrichment. Different colors represent different functional classifications. C. Scatterplot of enriched Kyoto Encyclopedia of Genes and Genomes (KEGG) pathways. The abscissa is the ratio of the number of differential genes annotated to the KEGG pathway to the total number of differential genes, and the ordinate is the KEGG pathway.

Table 3. DEG analysis

| Gene ID | Gene name | Log2 (fold change) | P value | Gene biotype |
|---------------------|----------------------|--------------------|----------|----------------------|
| ENSMUSG00000086503 | <i>Xist</i> | -12.0327581 | 7.44E-23 | lincRNA |
| ENSMUSG00000069049 | <i>Eif2s3y</i> | 10.39694356 | 1.16E-16 | protein_coding |
| ENSMUSG00000069045 | <i>Ddx3y</i> | 10.11256552 | 3.76E-16 | protein_coding |
| ENSMUSG00000056673 | <i>Kdm5d</i> | 9.071396297 | 4.39E-13 | protein_coding |
| ENSMUSG00000068457 | <i>Uty</i> | 8.128248158 | 1.83E-10 | protein_coding |
| ENSMUSG00000035692 | <i>Isg15</i> | 2.190069626 | 2.12E-10 | protein_coding |
| ENSMUSG00000093954 | <i>Gm16867</i> | 2.151542912 | 2.41E-10 | protein_coding |
| ENSMUSG00000105703 | <i>Gm43305</i> | 5.098977247 | 2.71E-10 | processed_transcript |
| ENSMUSG00000087627 | <i>A230059L01Rik</i> | 8.037463385 | 4.54E-10 | processed_transcript |
| ENSMUSG00000014956 | <i>Ppp1cb</i> | 2.316868255 | 3.10E-09 | protein_coding |
| ENSMUSG00000036390 | <i>Gadd45a</i> | 2.738038721 | 7.22E-09 | protein_coding |
| ENSMUSG00000020490 | <i>Btnl10</i> | 2.80901585 | 1.17E-08 | protein_coding |
| ENSMUSG00000063856 | <i>Gpx1</i> | 2.235589039 | 3.90E-08 | protein_coding |
| ENSMUSG00000028328 | <i>Tmod1</i> | 3.339863428 | 4.43E-08 | protein_coding |
| ENSMUSG000000089827 | <i>1700023H06Rik</i> | 2.522120464 | 6.57E-08 | processed_transcript |
| ENSMUSG000000025498 | <i>Irf7</i> | 1.719942337 | 7.82E-08 | protein_coding |
| ENSMUSG00000114540 | <i>Gm6421</i> | 1.92761716 | 2.03E-07 | processed_pseudogene |
| ENSMUSG00000027556 | <i>Car1</i> | 2.198020891 | 2.15E-07 | protein_coding |
| ENSMUSG00000039166 | <i>Akap7</i> | 2.661064637 | 2.61E-07 | protein_coding |
| ENSMUSG00000044352 | <i>Sowaha</i> | 4.851550147 | 3.06E-07 | protein_coding |
| ENSMUSG000000062198 | <i>2700097O09Rik</i> | 2.861887771 | 4.54E-07 | protein_coding |
| ENSMUSG00000064215 | <i>Ifi27</i> | 2.558643976 | 4.67E-07 | protein_coding |
| ENSMUSG00000028124 | <i>Gclm</i> | 2.690375571 | 4.73E-07 | protein_coding |
| ENSMUSG00000032745 | <i>Gpbpl</i> | 1.701926246 | 5.07E-07 | protein_coding |
| ENSMUSG000000041777 | <i>Cir1</i> | 2.983734607 | 5.23E-07 | protein_coding |
| ENSMUSG000000049775 | <i>Tmsb4x</i> | 1.321645714 | 5.83E-07 | protein_coding |
| ENSMUSG000000035530 | <i>Eif1</i> | 1.454870134 | 6.29E-07 | protein_coding |
| ENSMUSG00000076612 | <i>Ighg2c</i> | 2.541790751 | 6.54E-07 | IG_C_gene |
| ENSMUSG00000056895 | <i>Hist3h2ba</i> | 2.181801183 | 7.14E-07 | protein_coding |

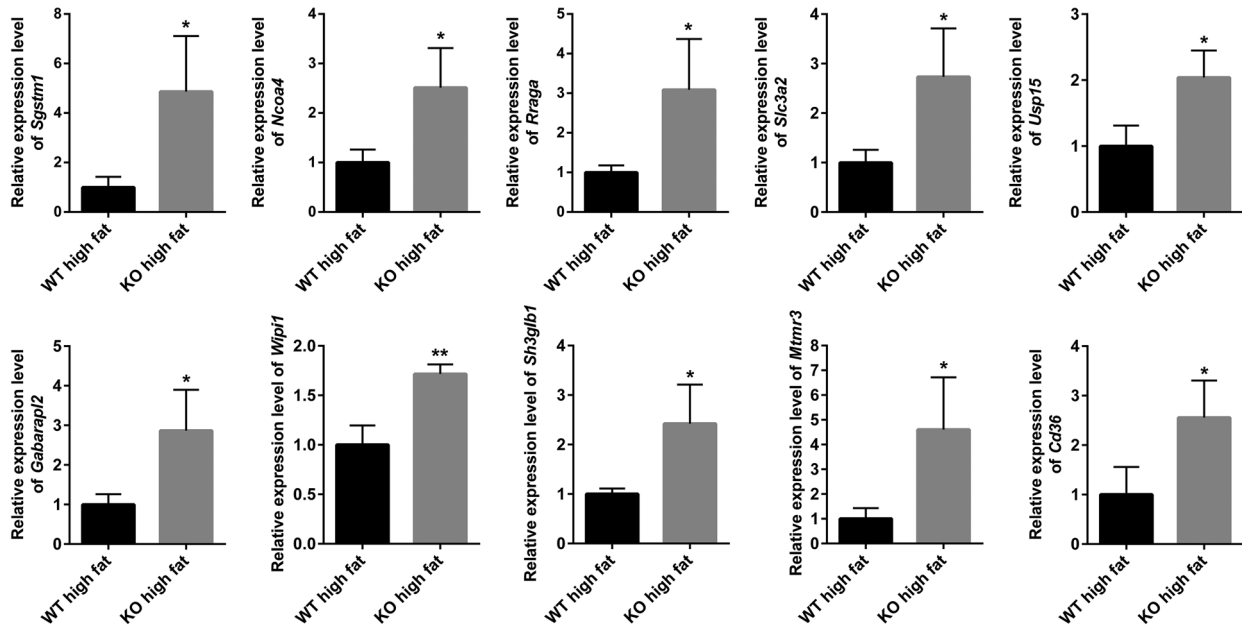


Fig. 5. Comparison of the expression levels of the ten genes of interest in peripheral blood. WT high fat: wild-type mouse high-fat diet (HFD) group. KO high fat: *Pdha1^{fl/fl}*Lyz2-Cre mouse HFD group. Data are shown as mean \pm SD values. Student's *t*-test was applied to comparisons between the two groups. * $P < 0.05$ compared with WT high fat. ** $P < 0.01$ compared with WT high fat.

animal, protein processing in endoplasmic reticulum, antigen processing and presentation, and chemical carcinogenesis.

Verification of RNA-seq results by qRT-PCR

We verified the blood mRNA levels of the genes sequenced in RNA-seq: sequestosome-1 (*Sgstm1*), nuclear receptor coactivator 4 (*Ncoa4*), Ras related GTP binding A (*Rraga*), solute carrier family 3 member 2 (*Slc3a2*), ubiquitin-specific peptidase 15 (*Usp15*), gamma-aminobutyric acid receptor-associated protein-like 2 (*Gabarapl2*), WD repeat domain, phosphoinositide-interacting 1 (*Wipi1*), SH3 domain containing Grb2 like endophilin B1 (*Sh3glb1*), myotubularin related protein 3 (*Mtmt3*), and cluster of differentiation (*Cd36*) by qRT-PCR. The changes in expression levels of the genes were consistent with the results obtained from the RNA-seq analysis (Fig. 5).

Discussion

Animal models have made an important contribution to description of the molecular mechanism of obesity. As PDH plays an important role in cell energy metabolism, a deficiency of PDH in humans results in lactic acidosis and neurological dysfunction, leading to death during infancy. Systemic knockout PDH mice are prone to death. Therefore, we constructed a mouse model of PDH-specific knockout in macrophages. Gene knockout technology can be used for site-specific integration of

foreign genes into the target cell genome through homologous recombination, which can replace the target sequence of the recipient cell genome to produce precise gene mutations and overcome the blindness and coincidence of random integration, without affecting gene sequences outside the target. This is the first time a mouse model of PDH-specific knockout in macrophages has been constructed, and the mice are breeding well.

The mitochondrial pyruvate dehydrogenase complex has been implicated as a central metabolic node that regulates the conversion of pyruvate into acetyl-CoA. Its dysfunction has been implicated in the development of diverse metabolic diseases. Our study showed that *Pdha1^{fl/fl}*Lyz2-Cre mice were more susceptible to HFD-induced obesity. Thus, we hypothesize that PDH is a protective factor based on this result; that is, it may play an important role in maintaining the normal metabolism of the body. This was consistent with a previous study showing that increased muscle PDH activity and glucose oxidation could promote glucose lowering and that whole-body deficiency of PDK4 in mice would improve glycemia during experimental obesity [13]. Furthermore, it also corresponded to a report that cardiac *Pdhal* deficiency caused a large myocardial infarct size and macrophage infiltration in the heart and sensitized the heart to the toxicological actions of ischemic stress [14].

KEGG analysis showed that the pathways of PDH were involved in ferroptosis, mitophagy-animal, cardiac muscle contraction, ECM-receptor interaction, glutathi-

one metabolism, ubiquitin mediated proteolysis, hematopoietic cell lineage, nitrogen metabolism, ether lipid metabolism, protein digestion and absorption, GABAergic synapse, drug metabolism-cytochrome P450, alcoholism, metabolism of xenobiotics by cytochrome P450, autoimmune thyroid disease, allograft rejection, autophagy-animal, protein processing in endoplasmic reticulum, antigen processing and presentation, chemical carcinogenesis. Based on the above pathways, we focused on the genes associated with ferroptosis and autophagy. Our study verified that the changes in expression levels of the genes *Sgstm1*, *Ncoa4*, *Rraga*, *Slc3a2*, *Usp15*, *Gabarapl2*, *Wipi1*, *Sh3glb1*, *Mtmr3*, and *Cd36* were consistent with the results obtained from our RNA-seq analysis.

There is some evidence regarding these genes and obesity in the recent literature. Lipid accumulation often leads to lipotoxic injuries in hepatocytes, which can cause nonalcoholic steatohepatitis. Increased activation of mechanistic target of rapamycin complex 1 (mTORC1) and stimulator of interferon gene 1 (*Sting1*) was observed in liver tissues of nonalcoholic fatty liver disease patients. The involvement of *Sting1* in mTORC1 activation was dependent on *Sgstm1*, a key regulator of the mTORC1 pathway [15]. Mice fed a high-fat diet can present decreased iron levels, endoplasmic reticulum stress, and impaired hepatic insulin signaling, while *Ncoa4* delivers ferritin to the lysosome and mediates the selective autophagic degradation of ferritin, playing a critical role in intracellular and systemic iron homeostasis. The overexpression of *Ncoa4* can improve endoplasmic reticulum stress and hepatic insulin resistance [16]. Obese mice fed an HFD showed a variety of defects in oocytes that influenced the offspring's tendency to develop metabolic disease. The expression of the autophagy-related gene *Rraga* was reduced in obese mice [17]. *Cd36*, which belongs to the class B scavenger receptors, is involved in various diseases and conditions, such as insulin resistance, atherosclerosis, and non-alcoholic fatty liver disease (NAFLD) [18].

Ferroptosis is an iron-dependent form of non-apoptotic cell death driven by the lipid peroxidation typically triggered by inhibiting antioxidant systems, in particular the cystine/glutamate antiporter and glutathione peroxidase 4 (GPX4) [19]. This process is characterized by the accumulation of lipid peroxidation products and lethal reactive oxygen species (ROS) derived from iron metabolism, and it can be pharmacologically inhibited by iron chelators and lipid peroxidation inhibitors. GPX4, heat shock protein beta-1, nuclear factor, and erythroid 2-related factor 2 function as the negative regulators of ferroptosis, while nicotinamide adenine

dinucleotide phosphate oxidase and *p53* act as the positive regulators of ferroptosis [20]. Recent studies have shown that ferroptosis is related to the pathophysiological processes of many diseases and conditions, such as tumors, cardiovascular diseases, nervous system diseases, ischemia-reperfusion injury, kidney injury, and blood diseases [21, 22]. Macrophages are involved in maintaining iron homeostasis in the body. In addition to the dietary iron absorbed from the intestine, most of the iron in the normal body comes from the phagocytic processing of aging red blood cells phagocytized by macrophages. An axis of hepcidin-ferroportin that maintains iron levels is present in organisms, and ferroportin (FPN) is present on the surface of macrophages cell membranes which regulate iron homeostasis. Hepcidin is a key factor in regulating FPN, which binds to FPN and mediates its internal degradation inactivation. Macrophages directly participate in the regulation of iron homeostasis through the hepcidin-FPN axis [23]. TCA cycle and mitochondrial electron transport chain (ETC) activity are required for the generation of sufficient lipid ROS to initiate ferroptosis. Pyruvate oxidation-mediated activation of the TCA cycle is necessary for fatty acid synthesis and subsequent lipid peroxidation, promoting ferroptosis. This glucose-mediated sensitization to ferroptosis induction relies on pyruvate oxidation catalyzed by PDH [24]. According to our KEGG analysis, ferroptosis exhibited a remarkable difference between the two HFD-fed groups. Expression of the genes *Slc3a2*, *Tfrc*, *Prnp*, *Gclm*, and *Ncoa4*, which are involved in ferroptosis, changed. Among these genes, *Slc3a2* plays a key role in driving the uptake of glutamine and leucine, which is critical for metabolic activation and cellular function [25]. *Ncoa4* is a selective cargo receptor. The phagocytosis of ferritin mediated by *ncoa4* can maintain iron homeostasis in the cell by depleting ferritin [26]. We verified that the changes in the expression levels of the genes *Slc3a2* and *Ncoa4* were consistent with the results from our RNA-seq analysis.

Autophagy, an important metabolic process of material flow within the cell, is mediated by vacuoles or lysosomes of eukaryotes. Some of the damaged proteins and organelles wrapped by the double-membrane structures of autophagy vesicles are sent into lysosomes to degrade and recycle. As an adaptive action of cells to various stress responses, autophagy is an important part of stress responses, such as endoplasmic reticulum stress, and has a certain relationship with the onset of metabolic syndrome [27]. The formation of autophagosomes is accompanied by the conversion of LC3 I to LC3 II. Thus, LC3 expression has also become a marker of autophagy, while the ratio of LC3 II/LC3 I represents the

level of autophagy [28]. When metabolic syndrome is present, autophagy can timely remove foreign bodies, promote lipid catabolism, and play a role in regulating lipid metabolism, insulin resistance, intracellular environmental stability, and oxidative stress by resisting lipid peroxidation stress, inflammatory stress, and other adverse conditions [29]. In metabolic stress states such as energy deficiency, an increase of AMP or ADP/ATP can lead to the activation of AMPK, thus promoting the initiation of autophagy. Dysfunctions of autophagy and apoptosis are involved in the mitochondrial dysfunction in the non-alcoholic fatty liver [30]. PDK4 inhibits the nuclear translocation of the transcription factor EB, thus inhibiting lysosomal function. These changes result in the interruption of autophagic flux [31]. In this study, we focused on the remarkable difference in autophagy between the two HFD groups according to our KEGG analysis, and we verified that the changes in the expression levels of the genes *Rraga*, *Mtmt3*, *Gabarapl2*, and *Sgstml* were consistent with the results of our RNA-seq analysis.

Interestingly, autophagy, the stress-responsive catabolic pathway, can also promote ferroptosis by degrading the iron-storage protein ferritin and thus increase the cellular iron concentration [32]. When the intracellular iron level is reduced, *Ncoa4* can enhance the autophagy pathway of ferritin to increase the intracellular free iron level and induce cell ferroptosis. Specific knockout of the *Ncoa4* gene can inhibit the autophagy of ferritin and effectively prevent the occurrence of ferroptosis [33, 34]. In addition, it has been reported that the knockout of encoding autophagy-related 5 and encoding autophagy-related 7 in mice embryonic fibroblasts induced ferroptosis [35]. Therefore, autophagy may promote ferroptosis. Some researchers also believe that ferroptosis is a type of autophagy-dependent cell death [36]. In our study, we confirmed that the knockout of *Pdhal* could up-regulate some genes related with ferroptosis and autophagy, providing the basis for the further study of *Pdhal* function in the future.

In summary, *Pdhal^{fl/fl}Lyz2-Cre* mice could reproduce the phenotype changes in obesity. The present study analyzed the whole-genome expression of HFD *Pdhal^{fl/fl}Lyz2-Cre* mice by RNA-seq technique and transcriptional changes of a series of genes involved in several pathways. We verified that the changes in the expression levels of the genes *Sgstml*, *Ncoa4*, *Rraga*, *Slc3a2*, *Usp15*, *Gabarapl2*, *Wip1*, *Sh3glb1*, *Mtmt3*, and *Cd36* were consistent with the experimental results from our RNA-seq analysis. It remains unknown what the net regulatory effect is of the up- and down-regulation of the above genes. However, it is clear that the application of

this *Pdhal^{fl/fl}Lyz2-Cre* mouse model to exploration of the relationships between *Pdhal* and the development of HFD-induced obesity will play a very important role in the formulation of treatment strategies for PDH-related diseases.

Funding

This study was supported by the National Natural Science Foundation of China (Grant No. 91739119, 81670698, 81670406).

Ethics Approval

The animal experiments were approved by the ethics committee of Dalian Medical University (No. AEE19093).

Acknowledgments

The authors declare that they have no competing interests.

References

1. Singh RK, Kumar P, Mahalingam K. Molecular genetics of human obesity: A comprehensive review. *C R Biol.* 2017; 340: 87–108. [Medline] [CrossRef]
2. Iizuka Y, Kim H, Nakasatomi M, Matsumoto A, Shimizu J. Phenotypic and genotypic changes in obesity and type 2 diabetes of male KK mice with aging. *Exp Anim.* 2022; 71: 71–81. [Medline] [CrossRef]
3. Hwang J, Yoo JA, Yoon H, Han T, Yoon J, An S, et al. The role of leptin in the association between obesity and psoriasis. *Biomol Ther (Seoul).* 2021; 29: 11–21. [Medline] [CrossRef]
4. Vieira E, Mirizio GG, Barin GR, de Andrade RV, Nimer NFS, La Sala L. Clock genes, inflammation and the immune system—Implications for diabetes, obesity and neurodegenerative diseases. *Int J Mol Sci.* 2020; 21: 9743. [Medline] [CrossRef]
5. Ying W, Fu W, Lee YS, Olefsky JM. The role of macrophages in obesity-associated islet inflammation and β -cell abnormalities. *Nat Rev Endocrinol.* 2020; 16: 81–90. [Medline] [CrossRef]
6. Wang L, Hu J, Zhou H. Macrophage and adipocyte mitochondrial dysfunction in obesity-induced metabolic diseases. *World J Mens Health.* 2021; 39: 606–614. [Medline] [CrossRef]
7. Palmieri EM, Gonzalez-Cotto M, Baseler WA, Davies LC, Ghesquière B, Maio N, et al. Nitric oxide orchestrates metabolic rewiring in M1 macrophages by targeting aconitase 2 and pyruvate dehydrogenase. *Nat Commun.* 2020; 11: 698. [Medline] [CrossRef]
8. Ali L, Schnitzler JG, Kroon J. Metabolism: The road to inflammation and atherosclerosis. *Curr Opin Lipidol.* 2018; 29: 474–480. [Medline] [CrossRef]
9. Sun J, Li J, Guo Z, Sun L, Juan C, Zhou Y, et al. Overexpression of pyruvate dehydrogenase E1 α subunit inhibits Warburg effect and induces cell apoptosis through mitochondria-mediated pathway in hepatocellular carcinoma. *Oncol Res.* 2019; 27: 407–414. [Medline] [CrossRef]

10. Thoudam T, Ha CM, Leem J, Chanda D, Park JS, Kim HJ, et al. PDK4 augments ER-mitochondria contact to dampen skeletal muscle insulin signaling during obesity. *Diabetes*. 2019; 68: 571–586. [[Medline](#)] [[CrossRef](#)]
11. Ma WQ, Sun XJ, Wang Y, Zhu Y, Han XQ, Liu NF. Restoring mitochondrial biogenesis with metformin attenuates β -GP-induced phenotypic transformation of VSMCs into an osteogenic phenotype via inhibition of PDK4/oxidative stress-mediated apoptosis. *Mol Cell Endocrinol*. 2019; 479: 39–53. [[Medline](#)] [[CrossRef](#)]
12. Min BK, Oh CJ, Park S, Lee JM, Go Y, Park BY, et al. Therapeutic effect of dichloroacetate against atherosclerosis via hepatic FGF21 induction mediated by acute AMPK activation. *Exp Mol Med*. 2019; 51: 1–12. [[Medline](#)] [[CrossRef](#)]
13. Al Batran R, Gopal K, Capozzi ME, Chahade JJ, Saleme B, Tabatabaei-Dakhili SA, et al. Pimozide alleviates hyperglycemia in diet-induced obesity by inhibiting skeletal muscle ketone oxidation. *Cell Metab*. 2020; 31: 909–919.e8. [[Medline](#)] [[CrossRef](#)]
14. Sun W, Quan N, Wang L, Yang H, Chu D, Liu Q, et al. Cardiac-specific deletion of the *Pdha1* gene sensitizes heart to toxicological actions of ischemic stress. *Toxicol Sci*. 2016; 151: 193–203. [[Medline](#)] [[CrossRef](#)]
15. Liu K, Qiu D, Liang X, Huang Y, Wang Y, Jia X, et al. Lipotoxicity-induced STING1 activation stimulates MTORC1 and restricts hepatic lipophagy. *Autophagy*. 2022; 18: 860–876. [[Medline](#)] [[CrossRef](#)]
16. Jiang C, Zhang S, Li D, Chen L, Zhao Y, Mei G, et al. Impaired ferritinophagy flux induced by high fat diet mediates hepatic insulin resistance via endoplasmic reticulum stress. *Food Chem Toxicol*. 2020; 140: 111329. [[Medline](#)] [[CrossRef](#)]
17. Pan MH, Zhu CC, Ju JQ, Xu Y, Luo SM, Sun SC, et al. Single-cell transcriptome analysis reveals that maternal obesity affects DNA repair, histone methylation, and autophagy level in mouse embryos. *J Cell Physiol*. 2021; 236: 4944–4953. [[Medline](#)] [[CrossRef](#)]
18. Liu J, Yang P, Zuo G, He S, Tan W, Zhang X, et al. Long-chain fatty acid activates hepatocytes through CD36 mediated oxidative stress. *Lipids Health Dis*. 2018; 17: 153. [[Medline](#)] [[CrossRef](#)]
19. Le Y, Zhang Z, Wang C, Lu D. Ferroptotic cell death: new regulatory mechanisms for metabolic diseases. *Endocr Metab Immune Disord Drug Targets*. 2021; 21: 785–800. [[Medline](#)] [[CrossRef](#)]
20. Xie Y, Hou W, Song X, Yu Y, Huang J, Sun X, et al. Ferroptosis: process and function. *Cell Death Differ*. 2016; 23: 369–379. [[Medline](#)] [[CrossRef](#)]
21. Capelletti MM, Manceau H, Puy H, Peoc'h K. Ferroptosis in liver diseases: an overview. *Int J Mol Sci*. 2020; 21: 4908. [[Medline](#)] [[CrossRef](#)]
22. Li J, Cao F, Yin HL, Huang ZJ, Lin ZT, Mao N, et al. Ferroptosis: past, present and future. *Cell Death Dis*. 2020; 11: 88. [[Medline](#)] [[CrossRef](#)]
23. Cornelissen A, Guo L, Sakamoto A, Virmani R, Finn AV. New insights into the role of iron in inflammation and atherosclerosis. *EBioMedicine*. 2019; 47: 598–606. [[Medline](#)] [[CrossRef](#)]
24. Song X, Liu J, Kuang F, Chen X, Zeh HJ 3rd, Kang R, et al. PDK4 dictates metabolic resistance to ferroptosis by suppressing pyruvate oxidation and fatty acid synthesis. *Cell Rep*. 2021; 34: 108767. [[Medline](#)] [[CrossRef](#)]
25. Terrén I, Orrantia A, Vitallé J, Zenarruzabeitia O, Borrego F. NK cell metabolism and tumor microenvironment. *Front Immunol*. 2019; 10: 2278. [[Medline](#)] [[CrossRef](#)]
26. Quiles Del Rey M, Mancias JD. NCOA4-mediated ferritinophagy: a potential link to neurodegeneration. *Front Neurosci*. 2019; 13: 238. [[Medline](#)] [[CrossRef](#)]
27. Sung KC, Lee MY, Kim YH, Huh JH, Kim JY, Wild SH, et al. Obesity and incidence of diabetes: Effect of absence of metabolic syndrome, insulin resistance, inflammation and fatty liver. *Atherosclerosis*. 2018; 275: 50–57. [[Medline](#)] [[CrossRef](#)]
28. Kabeya Y, Mizushima N, Ueno T, Yamamoto A, Kirisako T, Noda T, et al. LC3, a mammalian homologue of yeast Apg8p, is localized in autophagosomal membranes after processing. *EMBO J*. 2000; 19: 5720–5728. [[Medline](#)] [[CrossRef](#)]
29. Li RH, Yu L, Miao P, Ding X, Sun B, Feng X. [Changes in expression of autophagy-related proteins, Beclin-1 and LC3, and effects of rapamycin on their expression in hypoxic-ischemic hippocampus]. *Zhongguo Dang Dai Er Ke Za Zhi*. 2015; 17: 400–404. [[Medline](#)]
30. Cui P, Hu W, Ma T, Hu M, Tong X, Zhang F, et al. Long-term androgen excess induces insulin resistance and non-alcoholic fatty liver disease in PCOS-like rats. *J Steroid Biochem Mol Biol*. 2021; 208: 105829. [[Medline](#)] [[CrossRef](#)]
31. Ma WQ, Sun XJ, Zhu Y, Liu NF. PDK4 promotes vascular calcification by interfering with autophagic activity and metabolic reprogramming. *Cell Death Dis*. 2020; 11: 991. [[Medline](#)] [[CrossRef](#)]
32. Gao M, Monian P, Pan Q, Zhang W, Xiang J, Jiang X. Ferroptosis is an autophagic cell death process. *Cell Res*. 2016; 26: 1021–1032. [[Medline](#)] [[CrossRef](#)]
33. Mancias JD, Wang X, Gygi SP, Harper JW, Kimmelman AC. Quantitative proteomics identifies NCOA4 as the cargo receptor mediating ferritinophagy. *Nature*. 2014; 509: 105–109. [[Medline](#)] [[CrossRef](#)]
34. Lu B, Chen XB, Ying MD, He QJ, Cao J, Yang B. The role of ferroptosis in cancer development and treatment response. *Front Pharmacol*. 2018; 8: 992. [[Medline](#)] [[CrossRef](#)]
35. Hou W, Xie Y, Song X, Sun X, Lotze MT, Zeh HJ 3rd, et al. Autophagy promotes ferroptosis by degradation of ferritin. *Autophagy*. 2016; 12: 1425–1428. [[Medline](#)] [[CrossRef](#)]
36. Zhou B, Liu J, Kang R, Klionsky DJ, Kroemer G, Tang D. Ferroptosis is a type of autophagy-dependent cell death. *Semin Cancer Biol*. 2020; 66: 89–100. [[Medline](#)] [[CrossRef](#)]